Binding of glycosaminoglycan saccharides to hydroxyapatite surfaces: A density functional theory study

Ian Streeter[1,2], **Nora H. de Leeuw**[1,2]

[1] Department of Chemistry, University College London, 20 Gordon Street, London, United Kingdom WC1H 0AJ.

[2] Insitute of Orthopaedics & Musculoskeletal Science, University College London, Brockley Hill, Stanmore, United Kingdom HA7 4LP

Email: i.streeter@ucl.ac.uk; Fax: +44 (0)20 7679 7463

Abstract

Density functional theory calculations implemented by the SIESTA code are used to study the interactions of the saccharides *N*-acetylgalactosamine (GalNAc) and glucuronic acid (GlcA) with the (0001) and (01$\bar{1}$0) surfaces of the mineral hydroxyapatite (HAP). GalNAc and GlcA are the constituent monosaccharides of chondroitin, which is a glycosaminoglycan found in bone and cartilage, and whose interactions with HAP have been implicated as a controlling factor in the process of biomineralisation. Geometry optimisation calculations are used to identify low energy adsorption structures of the monosaccharides on the HAP surfaces, and to calculate the corresponding adsorption energies. The calculations show that GalNAc interacts with HAP principally through its hydroxy and acetyl amine functional groups, and deprotonated GlcA interacts principally through its hydroxy and carboxylate functional groups. The mode and strength of adsorption depends on the orientation of the saccharide with respect to the HAP surface, which has implications for the structural conformation of chondroitin chains in the presence of hydroxyapatite. Both monosaccharides bind more strongly to the (01$\bar{1}$0) surface than to the (0001) surface.

1 Introduction

Natural bone is a composite material, comprising a mineral phase, an organic phase and water (Currey 1998, Weiner & Wagner 1998, Fratzl *et al.* 2004). The mineral component, which is essential for the bone's stiffness, is present as nano-sized platelets of hydroxyapatite (HAP), $Ca_{10}(PO_4)_6(OH)_2$ (Kay *et al.* 1964), although with a varying degree of carbonate substitutions. In this paper we are concerned with the interaction of HAP crystals with a class of organic polysaccharides known as glycosaminoglycans (GAGs) (Kjellén & Lindahl 1991). GAGs are long unbranched chains of repeating disaccharide units, which have a high anionic charge in aqueous solution due to the deprotonation of carboxylic acid groups. The GAGs in bone are found as part of a proteoglycan, which is a macromolecule containing a core protein with one or more covalently attached GAGs, each containing typically 20–60 disaccharide units per chain.

Proteoglycans have been implicated in the role of regulating mineral deposition and crystal morphology in cartilage and in bone (Hunter 1991, Boskey 1992, Lamoureux *et al.* 2007), and it has been shown *in vitro* that GAGs have a strong regulatory effect on HAP crystallization (Rees *et al.* 2002, Hall *et al.* 1995, Okazaki *et al.* 1999). Furthermore, it has been shown using ^{31}P–^{13}C coupling in NMR experiments that HAP crystal surfaces in bone are predominantly in contact with GAGs, rather than with any other organic component (Wise *et al.* 2007). It is thought that GAGs can sequester calcium ions from aqueous solution due to their high negative charge, which could aid the process of HAP crystal nucleation. The preferential adsorption of GAGs on different surfaces of HAP could then control the rate and the direction of growth of the crystal (Hunter 1991, Boskey 1992). However, the complete process of mineralisation *in vivo* is still poorly understood, and is likely to be under the control of many different biomolecules and orchestrated by cells. The impetus for this study is that currently there is no detailed structural information on the adsorption modes of saccharides on HAP surfaces, which could help to elucidate the role of GAGs in the biomineralisation mechanism.

The predominant GAG found in bone and cartilage is chondroitin, which is illustrated in Figure 1a. Chondroitin is comprised of the two monosaccharides *N*-acetylgalactosamine (GalNAc) and glucuronic acid (GlcA), the latter of which is deprotonated in aqueous solution. The GalNAc saccharide is often sulphated on either one of its hydroxy groups, and so in a biological context the GAG is more commonly referred to as chondroitin sulphate, but we do not consider the effects of sulphation in the present study.

The structure of apatite surfaces has been investigated previously at high resolution using x-ray diffraction (Park *et al.* 2004, Pareek *et al.* 2007), showing that there is relaxation of the phosphate and calcium positions in the upper-most layers of the surface, compared with the bulk structure. Experimental studies using spectroscopic techniques have also demonstrated that apatite surfaces can significantly distort the conformations of adsorbed organic molecules such as proteins, as different regions of the molecule are attracted more strongly to the surface (Shaw *et al.* 2000, Long *et al.* 2001, Shaw *et al.* 2004, Capriotti *et al.* 2007, Shaw & Ferris 2008). The adsorption of a variety of organic molecules on apatite surfaces has been studied previously by computational techniques, including DFT (Almora-Barrios *et al.* 2009) and classical molecular dynamics (Mkhonto *et al.* 2006, Chen *et al.* 2007, Makrodimitris *et al.* 2007, Pan *et al.* 2007, de Leeuw & Rabone 2007, Almora-Barrios & de Leeuw 2010).

In this paper, we present a detailed computational study of the adsorption of the constituent monosaccharides of chondroitin to the surfaces of HAP. We have used density functional theory (DFT) to predict different modes of adsorption, and to provide quantitative information on the binding energies and interfacial interactions between the adsorbate and the apatite mineral. We consider the (0001) surface of HAP, which is the thermodynamically most stable surface (Mkhonto *et al.* 2006, Filgueiras *et al.* 2006), and the $(01\bar{1}0)$ surface, which is the dominant plane of HAP nanocrystals in a biological environment (Moradian-Oldak *et al.* 1991).

2 Methods

The DFT calculations presented in this paper were conducted using the SIESTA software package (Soler *et al.* 2002). This code uses a self-consistent density functional method using norm-conserving Trouiller-Martins pseudopotentials to describe the nucleus and core electrons (Troullier & Martins 1991) and a basis set of numerical atomic orbitals to describe valence electrons. The use of numerical atomic orbitals minimises any basis set superposition error (Inada & Orita 2008) and the SIESTA code is therefore particularly suitable for the investigation of adsorption energies; see for example Almora-Barrios *et al.* (2009) and Fernández *et al.* (2007). We have used the Perdew-Burke-Ernzerhof generalised gradients approximation to describe the exchange and correlation functionals (Perdew *et al.* 1996). The basis sets for the oxygen and hydrogen in the HAP hydroxy groups were obtained from the optimization of water at 0.2 GPa (Anglada *et al.* 2002, Junquera *et al.* 2001); the basis sets for the carbon, oxygen, nitrogen and hydrogen in the saccharides were optimized with respect to the interaction of guanine-cytosine at 0.2 GPa (Fernandez-Serra *et al.* 2000); and the basis sets for all other atoms used a double-ζ plus polarisation function. The unit cell was optimised using a cutoff energy of 250 Ry, sampling was taken at the Γ point, and a force tolerance of 0.01 eV Å^{-1} was used. This combination of basis sets and pseudopotentials has been used previously in studies of hydroxyapatite slabs, and it was shown that the energy was converged to within about 10 meV per unit cell, with errors of about 0.02 Å and 0.2° for the unit cell lengths and angles, respectively (Calderín & Stott 2003). These simulation parameters have also been used previously in studies of the adsorption of other organic molecules on HAP surfaces (Almora-Barrios *et al.* 2009, Almora-Barrios & de Leeuw 2010).

The HAP slabs simulated in this paper were taken from the surface structures that were identified in previous work (Filgueiras *et al.* 2006) using the METADISE code (Watson *et al.* 1996), and then optimised using SIESTA. In this structure the space group of bulk HAP is $P6_3/m$, as observed in crystallography (Kay *et al.* 1964), but with the unit cell doubled in the *b* direction so that it contains two columns of hydroxy groups, each running parallel to

the *c* axis. The hydroxy groups were arranged such that they were all oriented in the same direction within any one column, but alternating in direction between neighbouring columns. This arrangement of hydroxy groups has been shown to be the lowest energy configuration in DFT calculations of bulk HAP (de Leeuw 2001). The optimised parameters of the double unit cell are $a = 9.403$ Å, $2b = 18.812$ Å, $c = 6.954$ Å, $\alpha = \beta = 90°$, and $\gamma = 120°$. To create the slabs, this cell was doubled again to create a $(2 \times 2 \times 1)$ simulation supercell with the formula $Ca_{40}(PO_4)_{12}(OH)_4$, which previously has been shown to be sufficiently large that any further increase in the slab thickness had no significant effect on the calculated surface structure or adsorption energies of small organic molecules (Almora-Barrios *et al.* 2009). Three-dimensional periodic boundary conditions were used to create an infinitely repeating surface, and the slabs were separated from their images in neighbouring cells by a vacuum region of approximately 50 Å, thus avoiding interactions between repeating cells.

We have used two different slabs for the adsorption calculations in this paper, corresponding to the (0001) and $(01\bar{1}0)$ surfaces. The $(01\bar{1}0)$ slab has a different surface termination on each of its two faces, because it is not possible to construct a $(01\bar{1}0)$ with the same termination on both faces. Therefore, we have calculated the adsorption of the saccharides on both possible faces of this slab, and we refer to these surfaces in this paper as $(01\bar{1}0)$a and $(01\bar{1}0)$b.

Following the approach by Tasker (1979), the HAP surface slabs were created in such a way that no dipole was present in the *c*-direction of the simulation cell, which would have led to unphysical results. Upon adsorption of the organic molecule, a dipole could be introduced across the slab, which could not be corrected for using version 2.0.2 of the SIESTA code. However, the introduced dipole is not a property of the surface and is unlikely to have an effect on either the adsorption structures or energies. In particular, it is unlikely to affect the relative energies between different adsorption configurations, which is the principal focus of the present research.

The monosaccharides *N*-acetylgalactosamine and glucuronic acid were both optimised *in vacuo* using SIESTA. Each saccharide was modelled as the D-enantiomer and the α-

anomer, which is the biologically important configuration, and they were optimised in their lowest energy chair conformations. To replicate the effects of a long chain of chondroitin, and to prevent the presence of too many polar hydroxy groups, GalNAc was methylated on its 1- and 3- oxygen atoms, and GlcA was methylated on its 1- and 4- oxygen atoms, as shown in Figure 1; these are the oxygen atoms by which the monosaccharides condense into the chondroitin polymer. The GlcA molecule was optimised in two different forms, and in each case the carboxylic acid group was deprotonated. Firstly, it was optimised as a neutral complex with a sodium atom, and this structure was later used to calculate adsorption energies; and secondly it was optimised as a charged anion, and this structure was later used to calculate the deformation energy of the saccharide upon adsorption (*vide infra*). Conversely, GalNAc is an uncharged molecule, so the same optimised structure was used for all further calculations.

The input structures for the DFT optimisations of the adsorption structures were selected from the output of a separate series of coordinate optimisations based on classical interatomic potentials. The classical coordinate optimisations identified a large number of different adsorption conformations, with the monosaccharides in a range of different positions and orientations on the crystal surfaces. The hydroxyapatite was described by an interatomic potential model that accurately reproduces experimental properties of the crystal (de Leeuw 2004), and the saccharides GalNAc and GlcA were described by the GLYCAM06 forcefield, which is commonly used for carbohydrates (Kirschner *et al.* 2008). The software DL_POLY_2 was used to optimise the classical structures (Smith & Forester 1996).

Having identified possible low energy conformations using interatomic potentials, two conformations were chosen for each monosaccharide and for each HAP surface for further coordinate optimisation by DFT calculations in SIESTA. The chosen starting conformations corresponded to the predicted overall lowest energy adsorption, and the predicted lowest energy adsorption in which the saccharide was ‘upside down’ on the surface; that is to say the two chosen structures had opposite faces of the saccharide’s ring oriented towards the HAP surface.

For adsorptions of GlcA on HAP, a sodium cation was added to the simulation cell to counteract the negative charge of the deprotonated carboxylic acid. The GlcA molecule and the sodium were placed on opposite faces of the HAP slab, to minimise the sodium's effect on the saccharide's adsorption conformation.

The adsorption energies, E_{ads}, of the monosaccharides on the HAP surfaces were calculated as follows:

$$E_{\text{ads}} = E_{\text{system}} - (E_{\text{sacc}} - E_{\text{surf}}) \tag{1}$$

where E_{sacc} is the energy of the optimised saccharide *in vacuo*, E_{surf} is the energy of the optimised HAP surface in the absence of any adsorbate, and E_{system} is the combined energy of the HAP surface with an adsorbed saccharide. For GlcA, the term E_{sacc} refers to the energy of the sodium complex of the GlcA anion, and so the value of E_{ads} refers to the adsorption of this complex, with the anion and cation on opposite faces of the HAP slab. Note that it is not possible to further partition this adsorption energy to yield the individual contributions from the GlcA anion and the sodium cation.

For each DFT optimisation of a saccharide adsorbed onto a HAP surface, two further DFT calculations were performed with SIESTA. Firstly, the energy of the saccharide was calculated in its adsorbed conformation but in the absence of HAP (i.e. *in vacuo*); this energy was then compared to the energy of the relaxed saccharide *in vacuo*. Secondly, the energy of the HAP slab was calculated in the absence of the saccharide; this energy was compared to the energy of the relaxed slab. These calculations tell us how much energy it has cost to deform the surface and the adsorbate in the process of adsorption, which therefore allows a calculation of the strength of the attraction between the two phases after subtraction of these deformation energies.

3 Results and discussion

Figure 2 shows the optimised structures of the monosaccharides GalNAc and GlcA *in vacuo*. Both molecules are in the low enery chair conformation, with the majority of ring sub-

stituents in the more favourable equatorial positions. On each saccharide two of the hydroxy groups have been methylated to replicate their location within a long chain of chondroitin. The methylated GalNAc has two further hydroxy groups: one in the axial position at C4 (using the numbering system shown in Figure 1), and one at C6, which is conformationally flexible because it is not directly on the ring. The methylated GlcA also has two hydroxy groups, which are both in equatorial positions at the C2 and C3 positions. Finally, the *N*-acetyl amine group of GalNAc is in the C2 position, and the carboxylic acid group of GlcA is in the C5 position.

Figure 3 shows the structures of the two HAP slabs used in this study in the absence of any adsorbate, which have been optimised in SIESTA and are described in detail in previous work (Almora-Barrios *et al.* 2009). The slabs consist of calcium cations, tetrahedral phosphate groups and hydroxy groups. The (0001) surface shown in Figure 3a has a hexagonal arrangement, with the hydroxy groups arranged in columns perpendicular to the surface. In the $(01\bar{1}0)$ surface shown in Figure 3c, the columns of hydroxy groups lie parallel to the surface plane, but the orientation of the hydroxy groups themselves are distorted due to relaxation of the surface. The top and bottom surfaces of the slab in Figure 3c are not identical, and it is not possible to create an $(01\bar{1}0)$ surface with equal terminations on both faces. In this paper, we use the term $(01\bar{1}0)$a to describe the face of the slab that is furthest from the hydroxy groups (the lower face in Figure 3d) , and $(01\bar{1}0)$b to describe the face that contains the hydroxy groups (the upper face in Figure 3d), where adsorption of the saccharides is studied on both the 'a' and the 'b' faces. The structures of the relaxed slabs are consistent with experimental x-ray diffraction experiments of apatite surfaces, which demonstrate a rotation of the upper-most phosphate groups in the surface relative to the bulk structure (Park *et al.* 2004, Pareek *et al.* 2007).

3.1 Adsorption of methylated *N*-acetylgalactosamine

For each of the three surfaces of interest, the methylated GalNAc molecule was placed on the HAP slab in two different orientations, each one with a different face of the saccharide ring

in contact with the surface, and the system was geometry-optimised using SIESTA. There was movement of the atoms both in the HAP surface and in the adsorbate as the system approached its local minimum and favourable adsorption interactions were formed. Because only one trial conformation was minimised in SIESTA for each surface and for each orientation of the saccharide, it is possible that the optimised structures are not in their global energy minimum. However, the starting conformations had been chosen from extensive umbrella sampling using interatomic potentials, as described in Section 2, and so the optimised structures are likely to be good estimates of the lowest energy adsorption modes in terms of the principal interactions between the surface and the adsorbate.

In all of the adsorption conformations studied, the plane of the saccharide ring was oriented approximately parallel to the HAP surface. In the following discussion, an adsorption is described as 'orientation I' when the face of the GalNAc ring containing the 4-hydroxy group is oriented towards the surface, and 'orientation II' when the opposite face of the ring is oriented towards the surface, with the 4-hydroxy group pointing away from the surface.

Figure 4 shows the optimised adsorption of GalNAc in both orientations on the $(01\bar{1}0)$b surface; the equivalent images of adsorptions on the (0001) and $(01\bar{1}0)$a surfaces are shown in the Supporting Information. For all of the studied adsorptions of GalNAc on HAP, Figure 5 shows in detail the strongest interactions between the surface atoms and the polarised atoms of the saccharide (i.e. any oxygen, nitrogen, or hydrogen attached to an electronegative atom).

Table 1 lists the adsorption energies for each of the adsorption configurations in Figure 5. Also shown are the calculated energies of deformation of the HAP slab and the GalNAc molecule upon adsorption of the saccharide, as described in Section 2.

For all three HAP surfaces, the adsorption energy of GalNAc was lower when the molecule was in orientation I rather than in orientation II. Comparing the energies in Table 1 for the system with orientation I, the strength of adsorption on the different surfaces has the order $(01\bar{1}0)$b>$(01\bar{1}0)$a>(0001). This order is consistent with previous computational studies of the order of adsorption of other organic molecules on the (0001) and $(01\bar{1}0)$b surfaces

(Almora-Barrios *et al.* 2009), and it is consistent with the trend that is observed for the thermodynamic stabilities of the surfaces (Filgueiras *et al.* 2006), where the less stable surfaces are more reactive towards adsorbing species (de Leeuw & Rabone 2007).

It can be seen in Figure 4 that in orientation I both hydroxy groups of GalNAc point directly towards the HAP surface, where they form strong hydrogen bonds to the surface phosphate groups. Conversely, the 4-hydroxy group points away from the surface in orientation II, and this effect was observed on all surfaces of HAP (see Figure 5 and the Supporting Information). The 6-hydroxy group is conformationally flexible because it is not located immediately on the ring, and so it is able to form a hydrogen bond to the surface in either orientation, but the 4-hydroxy group is located directly on the ring and it therefore has limited ability to point towards the surface. The absence of a second hydroxy-phosphate interaction is likely to be the most significant reason that GalNAc had a clearly preferred orientation on all three surfaces.

From Figure 5 it can be seen that in all of the optimised structures the surface atoms interact primarily with the saccharide hydroxy groups and acetyl amine group. Conversely, the ring oxygen and the methylated oxygens often do not form strong interactions with the surface, or only form long-range interactions. The hydroxy groups of HAP do not interact with the saccharide at all in the (0001) and $(01\bar{1}0)$a adsorptions, but only in the $(01\bar{1}0)$b adsorptions, for which the HAP hydroxy groups lie closer to the surface and were significantly distorted by the presence of the saccharide (e.g. in Figure 4a).

In the optimised adsorption of orientation I on the $(01\bar{1}0)$b surface, a proton was transferred from the 4-hydroxy group of GalNAc to a phosphate oxygen in the HAP surface (Figure 5c). Upon geometry optimisation of this orientation, the proton moved to be closer to the phosphate oxygen (1.01 Å) than it was to the saccharide oxygen (1.65 Å), and the P–O bond of the phosphate group lengthened from 1.57 Å to 1.66 Å. This proton transfer led to an especially large adsorption energy of -481.01 kJ mol^{-1} (Table 1). Proton transfer was not observed on either the (0001) or $(01\bar{1}0)$a surfaces; nor was it observed in the adsorption of GalNAc in orientation II on the $(01\bar{1}0)$b surface. Chemisorption of an adsorbate (rather than

physisorption) is largely determined by the reactivity the surface, and so the proton transfer observed here indicates the heightened reactivity of the $(01\bar{1}0)$b surface compared to the other two surfaces. If, on the other hand, the surface was protonated already, for example through dissociative adsorption of water, prior work on the sorption of water and organics at iron oxide surfaces indicates that the saccharide would bind more weakly to an already protonated surface (de Leeuw & Cooper 2007).

The deformation energies in Table 1 show how much energy was required to distort the GalNAc molecule and the surface away from their ideal conformations. This energy was repaid upon adsorption because deformation of the molecule acted to align the atoms of the surface and the adsorbate such that stronger interactions could form. For the lowest energy adsorptions on the three surfaces (orientation I), the energy required for the distortion of both the HAP and the GalNac molecule decreases in the order $(01\bar{1}0)$b>$(01\bar{1}0)$a>(0001). This order reflects the order of the reactivity of the surfaces; the implication is that a greater distortion is found upon adsorption on more reactive surfaces, because the greater energy penalty is repaid by stronger favourable interfacial interactions. Similarly, the distortion energy of the saccharide is always greater in orientation I than in orientation II, which indicates that extra distortion is needed to optimise the interactions for two hydrogen bonds rather than just one. The distortion energy of the saccharide on the $(01\bar{1}0)$b surface is especially high (338.38 kJ mol^{-1}) but this energy term includes the removal of the proton from the 4-hydroxy group as it was transferred to the HAP phosphate group.

3.2 Adsorption of methylated glucuronic acid

The adsorption modes of the methylated deprotonated GlcA molecule were studied in a similar manner to the GalNAc molecule, as described in section 3.1. The deprotonated GlcA molecule was placed on one face of the HAP slab and the sodium cation was placed on the opposite face in a low energy position. For each surface of interest, the system was geometry optimised in SIESTA with the saccharide in two different starting orientations, each one with a different face of the saccharide ring in contact with the surface. In the

discussion that follows an adsorption of GlcA is described as ‘orientation I’ when the face of the molecule containing the carboxylate and 3-hydroxy groups is oriented towards the surface, and ‘orientation II’ when this face is oriented away from the surface.

Figure 6 shows the optimised adsorption of GlcA in both orientations on the $(01\bar{1}0)$b surface; the equivalent images of adsorptions on the (0001) and $(01\bar{1}0)$a surfaces are shown in the Supporting Information. Figure 7 shows in detail the strongest interactions between the HAP surface atoms and the saccharide functional groups for all of the optimised structures. Table 2 is the equivalent of Table 1 but for adsorptions of GlcA; it shows the calculated adsorption energies and the calculated deformation energies of the HAP slab and the GlcA molecule upon adsorption on all three surfaces. For this saccharide, the calculated adsorption energy is the energy released when the sodium complex of the deprotonated saccharide molecule *in vacuo* is adsorbed onto the HAP slab, with the saccharide and the sodium occupying opposite surfaces (see Section 2).

In Figure 7 it can be seen that the surface atoms of hydroxyapatite principally interact with three different functional groups of GlcA: the carboxylate group and the two hydroxy groups. In particular, the two hydroxy groups tend to form hydrogen bonds to the surface phosphate groups, and the carboxylate group tends to interact with surface calcium ions. The other oxygen atoms in the GlcA molecule do not appear to interact with the surface so consistently in all of the adsorptions.

In all of the studied adsorptions of GlcA in orientation I, both of the hydroxy groups and the carboxylate group interact directly with the HAP surface (Figure 7). These three functional groups are all in equatorial positions when the GlcA molecule is in its lowest energy chair conformation, and for this reason they may all interact with the HAP surface in the orientation I adsorptions, even though the 2-hydroxy group is on the opposite face of the saccharide’s ring. This observation appears to remain valid even though the saccharide is not in a chair conformation in many of the adsorption structures.

In orientation II, the nature of the interactions are different on the different surfaces of HAP: on the (0001) surface both of the hydroxy groups and the carboxylate group interact

with the surface; but on the $(01\bar{1}0)$a surface the 3-hydroxy groups does not interact, and on the $(01\bar{1}0)$b surface the carboxylate group does not interact. It is more difficult for all three functional groups to interact with the surface when the molecule is in orientation II, because both the 3-hydroxy group and the carboxylate group are on the opposite face of the saccharide ring to the HAP, whereas in orientation I only one functional group is on the opposite face. However, the adsorption of orientation II on the (0001) surface (Figure 7d) confirms that it is still possible for all three functional groups to interact, at least under some circumstances. This pattern is in contrast with the adsorptions of the GalNAc molecule discussed in Section 3.1, for which the axial 4-hydroxy group was pointed away from the HAP surface in all of the orientation II adsorptions.

We acknowledge that the adsorption configurations of GlcA that we have identified here may not be the lowest energy adsorptions possible, and that the true global minima of orientation II on the $(01\bar{1}0)$ surfaces may involve all functional groups interacting with the surface, as was observed on the (0001) surface. However, it is likely to remain a significant observation that the functional groups of GlcA can interact with the surface more comfortably in orientation I than in orientation II, because of their locations on the different faces of the saccharide ring.

From Table 2 it can be seen that the adsorption of GlcA on the $(01\bar{1}0)$a and $(01\bar{1}0)$b surfaces are lower in energy for orientation I than for orientation II. However, for adsorption onto the (0001) where all three functional groups of interest interact with the surface in both orientations, orientation II was lower in energy, although the difference is small. Comparing the lowest energy orientation for all three surfaces, the calculated strength of adsorption decreases in the order $(01\bar{1}0)$b$>(01\bar{1}0)$a$>$(0001), although the difference between the latter two surfaces is small. This same order that was found in Section 3.1 for the adsorption of GalNAc. However, we acknowledge that when comparing between the surfaces, the adsorption energies in Table 2 have a contribution from the adsorption of the sodium ion, which is likely to have a different strength of adsorption to the different surfaces.

On the $(01\bar{1}0)$b surface, the adsorption of the GlcA molecule in orientation I led to proton

transfer from the 3-hydroxy group of the saccharide to a HAP phosphate group (Figure 7c). This is similar to the proton transfer described in Section 3.1, which was also on the $(01\bar{1}0)$b surface, which again it indicates the heightened reactivity of this surface compared to the other two surfaces. In the optimised structure, the proton is closer to the phosphate oxygen (1.04 Å) than it is to the saccharide oxygen (1.61 Å), and the P–O bond of the phosphate group is 1.69 Å, compared to 1.57 Å in the absence of adsorbate. This proton transfer is the reason for the anomalously high deformation energy and adsorption energy in Table 2 of the GlcA molecule in orientation I on the $(01\bar{1}0)$b surface.

Although the calculated adsorption energies of GlcA in Table 2 are typically larger than the equivalent adsorption energies of GalNAc in Table 1, caution should be taken when directly comparing these values, because those for the GlcA adsorptions include a contribution from the counter sodium ion. Similarly, the calculated deformation energies of the HAP slabs are larger for the GlcA adsorptions than for the GalNAc adsorptions, which, however, in the former case is probably due to both the saccharide and the sodium cation combining to disrupt to some extent the HAP structure on both faces of the slab.

3.3 Conclusions

The aim of this computer modelling study was to achieve a better understanding of the adsorption of the GAG chondroitin on hydroxyapatite surfaces. In this our first study, the simulations have focused on the single monosaccharides of chondroitin (*N*-acetylgalactosamine and deprotonated glucuronic acid), but which were methylated to retain the effect of a continuous chondroitin chain. The adsorptions of these monosaccharides were investigated on the (0001) surface of HAP and on two different variations of the $(01\bar{1}0)$ surface. Our simulations show that on all surfaces GalNAc interacts with HAP principally through its hydroxy and acetyl amine functional groups, and GlcA interacts principally through its hydroxy and carboxylate functional groups.

Apatite crystals *in vivo* are likely to contain step edges on the surfaces, which may affect the adsorption energies. Surface steps are less stable sites and hence more reactive, and it

is likely that GAGs would preferentially adsorb at step edges with correspondingly larger adsorption energies. For example, similar studies of the adsorption of organic molecules at planar and stepped surfaces of calcite and fluorite have shown that all adsorbates bind more strongly to the step edges than the surface terraces. The increase in binding energy was found to be dependent both on mineral composition and surface structure, as well as the geometry of the step edge and the surfactant (Cooper & de Leeuw 2002) and it is therefore difficult to estimate what their effect would be on the adsorption of the monosaccharide investigated here. However, it was also found that the adsorbate functional groups interacting with the planar surface were the same as those interacting with the step edges and as such is a property of the molecule rather than dependent on the surface structure (Cooper & de Leeuw 2004). As such, we expect that the monosaccharides in this study would interact with any surface defects in a similar fashion as on the planar surfaces studied here.

In aqueous solution, chondroitin tends to exist in helical conformations, because this maximises the number of intramolecular hydrogen bonds formed by the hydroxy groups between adjacent saccharides in the chain (Almond & Sheehan 2000). However, the present study has indicated that the hydroxy groups of the monosaccharides form strong hydrogen bonds to HAP phosphate groups, which implies that upon adsorption of a chondroitin chain, there will be competition for the saccharide hydroxy groups to form either intramolecular or interfacial hydrogen bonds. Hydrogen bonds to the phosphate groups are likely to be the stronger of the two, because of the higher negative charge of the surface oxygen. It is therefore likely that the interfacial interactions described in this investigation will dictate the mode of adsorption of long chains of chondroitin. In particular, we have shown that the monosaccharides have preferred orientations upon the HAP surface, and this preference makes it unlikely that chondroitin will retain its helical conformation upon adsorption.

The surface adsorption of GAGs on HAP in an aqueous environment is a competitive process between the functional groups of the saccharides and water molecules in forming interactions with the mineral. The DFT calculations presented in this paper were primarily concerned with determination of the chemical processes occurring between adsorbate and

surface, for which the inclusion of water molecules in the calculations was not required. Previous simulations of the adsorption of a tri-peptide molecule at the HAP surface, where *ab initio* calculations *in vacuo* and classical MD simulations *in vacuo* and in water were compared, have shown that the adsorption geometries and energies between DFT and classical MD *in vacuo* are consistent, but that water competes effectively with the adsorbates at the HAP (0001) surface, but not the $(01\bar{1}0)$ surface, where the peptide remains at the surface and its adsorption is strengthened further by an outer shell of water (Almora-Barrios & de Leeuw 2010). Furthermore, MD simulations of the adsorption of citric acid at the same HAP surfaces as studied here, have shown that the explicit inclusion of water led to a shift upwards in the binding energies of the citric acid to both surfaces as a result of the competitive adsorption of water, although the relevant binding energies between the surfaces remained very similar (de Leeuw & Rabone 2007). We may therefore expect that water would have a similar effect on the calculations in this study, namely that competing water may weaken the surface-adsorbate interaction, but that the $(01\bar{1}0)$ surface in any case remains more reactive towards the monosaccharides, which will remain bound to this surface.

Our simulations have shown that both monosaccharides studied have a strong preference for binding to the $(01\bar{1}0)$ surfaces (and in particular the $(01\bar{1}0)$b surface) rather than the (0001), whereas previous simulations suggest that even in the presence of competing water the $(01\bar{1}0)$ surface will remain reactive enough to ensure binding by organic adsorbates. This supports the observations made in natural bone that the nanocrystals of biological apatite are elongated along the *c*-axis, with a larger $(01\bar{1}0)$ surface area than any other surface (Moradian-Oldak *et al.* 1991). By preferentially adsorbing on the $(01\bar{1}0)$ surface, GAGs could stabilise that surface and inhibit further mineral deposition along the *a*- and *b*-axes. However, we note that many other organic molecules have also been shown to adsorb preferentially on the $(01\bar{1}0)$ surface (Mkhonto *et al.* 2006, Almora-Barrios *et al.* 2009, Almora-Barrios & de Leeuw 2010), and so GAGs are just one of many different classes of biomolecule that may be involved in controlling tissue mineralisation.

In future work, we plan to use DFT calculations to investigate how the sulphation of the

GalNAc monosaccharide affects its adsorption on HAP, because chondroitin in cartilage and bone is frequently sulphated at its various hydroxy groups (Lamoureux *et al.* 2007). We also plan to develop a classical model based on interatomic potentials to study HAP–saccharide interactions, using the electronic structure calculations in this work as a comparison. This will allow us to study larger systems that are beyond the scope of DFT calculations, including the adsorption of long chains of chondroitin, and the adsorption of saccharides in the presence of interfacial water using molecular dynamics simulations.

References

Almond, A. & Sheehan, J. K. 2000 Glycosaminoglycan conformation: do aqueous molecular dynamics simulations agree with x-ray fiber diffraction? *Glycobiology* **10**, 329–338.

Almora-Barrios, N., Austen, K. F. & de Leeuw, N. H. 2009 Density functional theory study of the binding of glycine, proline, and hydroxyproline to the hydroxyapatite (0001) and $(01\bar{1}0)$ surfaces. *Langmuir* **25**, 5018–5025.

Almora-Barrios, N. & de Leeuw, N. H. 2010 Modelling the interaction of a Hyp-Pro-Gly peptide with hydroxyapatite surfaces in aqueous environment. *CrystEngComm* **12**, 960–967.

Anglada, E, Soler, J. M., Junquera, J. & Artacho, E. 2002 Systematic generation of finite-range atomic basis sets for linear-scaling calculations. *Phys. Rev. B* **66**, 205101.

Boskey, A. L. 1992 Mineral–matrix interactions in bone and cartilage. *Clin. Orthop. Relat. Res.* **281**, 244–274.

Calderín, L. & Stott, M. J. 2003 Electronic and crystallographic structure of apatites. *Phys. Rev. B* **67**, 134106.

Capriotti, L. A., Beebe Jr., T. P. & Schneider, J. P. 2007 Hydroxyapatite surface-induced peptide folding. *J. Am. Chem. Soc.* **129**, 5281–5287.

Chen, X., Wang, Q., Shen, J., Pan, H. & Wu, T. 2007 Adsorption of leucine-rich amelogenin protein on hydroxyapatite (001) surface through -COO- claws. *J. Phys. Chem. C* **111**, 1284–1290.

Cooper, T. G. & de Leeuw, N. H. 2002 Co-adsorption of surfactants and water at inorganic solid surfaces. *Chem. Commun.* **14**, 1502–1503.

Cooper, T. G. & de Leeuw, N. H. 2004 A computer simulation study of sorption of model flotation reagents to planar and stepped 111 surfaces of calcium fluoride. *J. Mater. Chem.* **14**, 1927–1935.

Currey, J. D. 1998 Mechanical properties of vertebrate hard tissues. *P. I. Mech. Eng. H* **212**, 399–412.

de Leeuw, N. H. 2001 Local ordering of hydroxy groups in hydroxyapatite. *Chem. Commun.* **17**, 1646–1647.

de Leeuw, N. H. 2004 A computer modelling study of the uptake and segregation of fluoride ions at the hydrated hydroxyapatite (0001) surface: introducing $Ca_{10}(PO_4)_6(OH)_2$ potential model. *PCCP* **6**, 1860–1866.

de Leeuw, N. H. & Cooper, T. G. 2007 Surface simulation studies of the hydration of white rust $Fe(OH)_2$, goethite α-FeO(OH) and hematite α-Fe_2O_3. *Geochim. Cosmochim. Acta* **71**, 1655–1673.

de Leeuw, N. H. & Rabone, J. A. L. 2007 Molecular dynamics simulations of the interaction of citric acid with the hydroxyapatite (0001) and ($01\bar{1}0$) surfaces in an aqueous environment. *CrystEngComm* **9**, 1178–1186.

Fernández, E. M., Eglitis, R. I., Borstel, G. & Balbás, L. C. 2007 Ab initio calculations of H_2O and O_2 adsorption on Al_2O_3 substrates. *Comput. Mater. Sci.* **39**, 587–592.

Fernandez-Serra, M. V., Junquera, J., Jelsch, C., Lecomte, C. & Artacho, E. 2000 Electron density in the peptide bonds of crambin. *Solid State Commun.* **116**, 395–400.

Filgueiras, M. R. T, Mkhonto, D. & de Leeuw, N. H. 2006 Computer simulations of the adsorption of citric acid at hydroxyapatite surfaces. *J. Cryst. Growth* **294**, 60–68.

Fratzl, P., Gupta, H. S., Paschalis, E. P. & Roschger, P. 2004 Structure and mechanical quality of the collagen-mineral nano-composite in bone. *J. Mater. Chem.* **14**, 2115–2123.

Hall, R., Embery, G., Waddington, R. & Gilmour, A. 1995 The influence of fluoride on the adsorption of proteoglycans and glycosaminoglycans to hydroxyapatite. *Calcif. Tissue Int.* **56**, 236–239.

Hunter, G. K. 1991 Role of proteoglycan in the provisional calcification of cartilage – A review and reinterpretation. *Clin. Orthop. Relat. Res.* **262**, 256–280.

Inada, Y. & Orita, H. 2008 Efficiency of numerical basis sets for predicting the binding energies of hydrogen bonded complexes: Evidence of small basis set superposition error compared to Gaussian basis sets. *J. Comput. Chem.* **29**, 225–232.

Junquera, J., Paz, O., Sanchez-Portal, D. & Artacho, E. 2001 Numerical atomic orbitals for linear-scaling calculations. *Phys. Rev. B* **64**, 235111.

Kirschner, K. N., Yongye, A. B., Tschampel, S. M., González-Outeirño, J., Daniels, C. R., Foley, B. L. & Woods, R. J. 2008 GLYCAM06: A generalizable biomolecular force field. Carbohydrates. *J. Comput. Chem.* **29**, 622–655.

Kjellén, L. & Lindahl, U. 1991 Proteoglycans – structures and interactions. *Annu. Rev. Biochem.* **60**, 443–475.

Lamoureux, F., Baud'huin, M., Duplomb, L., Heymann, D. & Rédini, F. 2007 Proteoglycans: key partners in bone cell biology. *Bioessays* **29**, 758–771.

Long, J. R., Shaw, W. J., Stayton, P. S. & Drobny, G. P. 2001 Structure and dynamics of hydrated statherin on hydroxyapatite as determined by solid-state NMR. *Biochemistry* **40**, 15451–15455.

Makrodimitris, K., Masica, D. L., Kim, E. T. & Gray, J. J. 2007 Structure prediction of protein-solid surface interactions reveals a molecular recognition motif of statherin for hydroxyapatite. *J. Am. Chem. Soc.* **129**, 13713–13722.

Mkhonto, D., Ngoepe, P. E., Cooper, T. G. & de Leeuw, N. H. 2006 A computer modelling study of the interaction of organic adsorbates with fluorapatite surfaces. *Phys. Chem. Miner.* **33**, 314–331.

Moradian-Oldak, J., Weiner, S., Addadi, L., Landis, W. J. & Traub, W. 1991 Electron imaging and diffraction study of individual crystals of bone, mineralized tendon and synthetic carbonate apatite. *Connect. Tissue Res.* **25**, 219–228.

Okazaki, J., Embery, G., Hall, R. C., Hughes Wassell, D. T., Waddington, R. J. & Kamada, A. 1999 Adsorption of glycosaminoglycans onto hydroxyapatite using chromatography. *Biomaterials* **20**, 309–314.

Pan, H., Tao, J., Xu, X. & Tang, R. 2007 Adsorption processes of Gly and Glu amino acids on hydroxyapatite surfaces at the atomic level. *Langmuir* **23**, 8972–8981.

Pareek, A., Torrelles, X., Rius, J., Magdans, U. & Gies, H. 2007 Role of water in the surface relaxation of the fluorapatite (100) surface by grazing incidence x-ray diffraction. *Phys. Rev. B* **75**, 035148.

Park, C., Fenter, P., Zhang, Z., Cheng, L. & Sturchio, N. C. 2004 Structure of the fluorapatite (100)-water interface by high-resolution X-ray reflectivity. *Am. Mineral.* **89**, 1647–1654.

Perdew, J. P., Burke, K. & Ernzerhof, M. 1996 Generalized gradient approximation made simple. *Phys. Rev. Lett.* **77**, 3865–3868.

Kay, M. I., Young, R. A. & Posner, A. S. 1964 Crystal structure of hydroxyapatite. *Nature* **204**, 1050–1052.

Rees, S. G., Shellis, R. P. & Embery, G. 2002 Inhibition of hydroxyapatite crystal growth by bone proteoglycans and proteoglycan components. *Biochem. Biophys. Res. Commun.* **292**, 727–733.

Shaw, W. J., Long, J. R., Dindot, J. L., Campbell, A. A., Stayton, P. S. & Drobny, G. P. 2000 Determination of statherin N-terminal peptide conformation on hydroxyapatite crystals. *J. Am. Chem. Soc.* **122**, 1709–1716.

Shaw, W. J., Campbell, A. A., Paine, M. L. & Snead, M. L. 2004 The COOH terminus of the amelogenin, LRAP, is oriented next to the hydroxyapatite surface. *J. Biol. Chem.* **279**, 40263–40266.

Shaw, W. J. & Ferris, K. 2008 Structure, orientation, and dynamics of the C-terminal hexapeptide of LRAP determined using solid-state NMR. *J. Phys. Chem. B* **112**, 16975–16981.

Smith, W. & Forester, T. R. 1996 DL_POLY_2.0: A general-purpose parallel molecular dynamics simulation package. *J. Mol. Graphics* **14**, 136–141.

Soler, J. M., Artacho, E., Gale, J. D., García, A., Junquera, J., Ordejón, P. & Sánchez-Portal, D. 2002 The SIESTA method for ab initio order-*N* materials simulation. *J. Phys. Condens. Matter* **14**, 2745–2779.

Tasker, P. W. 1979 Surface energies, surface tensions and surface-structure of the alkali-halide crystals. *Philos. Mag. A* **39**, 119–136.

Troullier, N. & Martins, J. L. 1991 Efficient pseudopotentials for plane-wave calculations. *Phys. Rev. B* **43**, 1993–2006.

Watson, G. W., Kelsey, E. T., de Leeuw, N. H., Harris, D. J. & Parker, S. C. 1996 Atomistic simulation of dislocations, surfaces and interfaces in MgO. *J. Chem. Soc., Faraday Trans.* **9**, 433–438.

Weiner, S. & Wagner, H. D. 1998 The material bone: Structure mechanical function relations. *Annu. Rev. Mater. Sci.* **28**, 271–298.

Wise, E. R., Maltsev, S., Davies, M. E., Duer, M. J., Jaeger, C., Loveridge, N., Murray, R. C. & Reid, D. G. 2007 The organic-mineral interface in bone is predominantly polysaccharide. *Chem. Mater.* **19**, 5055–5057.

Tables

HAP surface	orientation	adsorption energy / kJ mol^{-1}	GalNAc deformation energy / kJ mol^{-1}	HAP deformation energy / kJ mol^{-1}
(0001)	I	-352.26	77.20	63.46
(0001)	II	-320.23	45.46	101.88
(01$\bar{1}$0)a	I	-451.63	109.48	113.81
(01$\bar{1}$0)a	II	-311.29	26.95	44.68
(01$\bar{1}$0)b	I	-481.01	338.38	207.99
(01$\bar{1}$0)b	II	-394.24	50.86	113.81

Table 1: Calculated adsorption energies and deformation energies of methylated *N*-acetylgalactosamine on hydroxyapatite surfaces.

HAP surface	orientation	adsorption energy / kJ mol^{-1}	GlcA deformation energy / kJ mol^{-1}	HAP deformation energy / kJ mol^{-1}
(0001)	I	-416.8	53.04	207.97
(0001)	II	-430.47	52.57	260.82
(01$\bar{1}$0)a	I	-436.42	115.61	366.35
(01$\bar{1}$0)a	II	-343.24	62.91	312.21
(01$\bar{1}$0)b	I	-698.67	341.05	310.53
(01$\bar{1}$0)b	II	-481.77	85.02	229.71

Table 2: Calculated adsorption energies and deformation energies of methylated deprotonated glucuronic acid on hydroxyapatite surfaces.

Figures

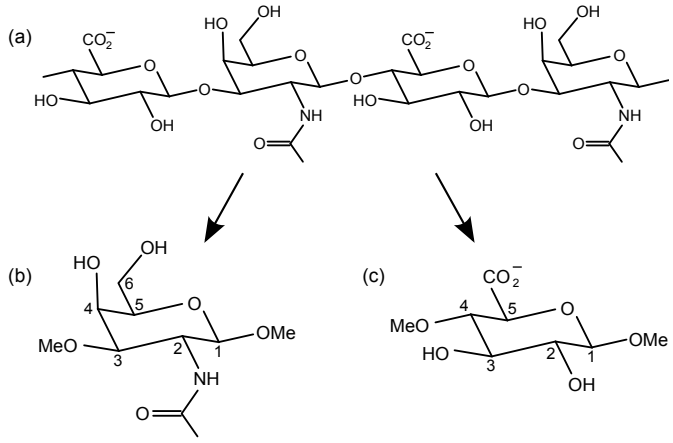

Figure 1: (a) A short chain of chondroitin, showing two disaccharide units. (b) Methylated acetylgalactosamine (GalNAc). (c) Methylated glucuronic acid (GlcA).

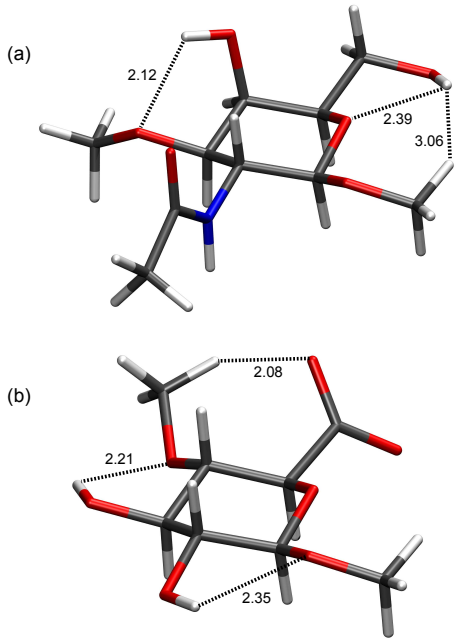

Figure 2: The lowest energy conformations of methylated GalNAc and GlcA *in vacuo* optimised by SIESTA (C = grey, O = red, N = blue, H = white. Intramolecular interaction distances are shown in Å.

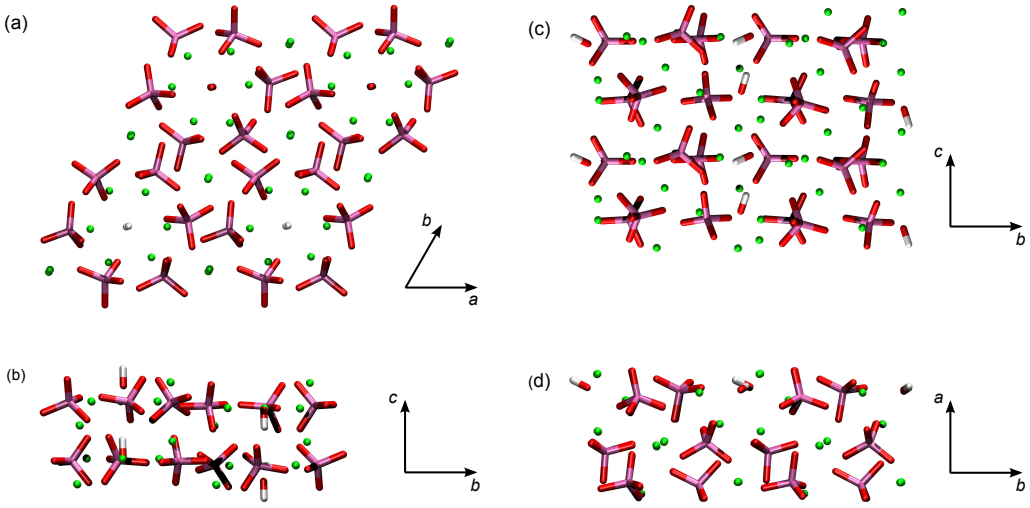

Figure 3: Relaxed slabs of hydroxyapatite: (a) plan view of the (0001) surface, (b) side view of the (0001) slab, (c) plan view of the $(01\bar{1}0)$ surface, (d) side view of the $(01\bar{1}0)$ slab (Ca = green, O = red, P = purple, H = white).

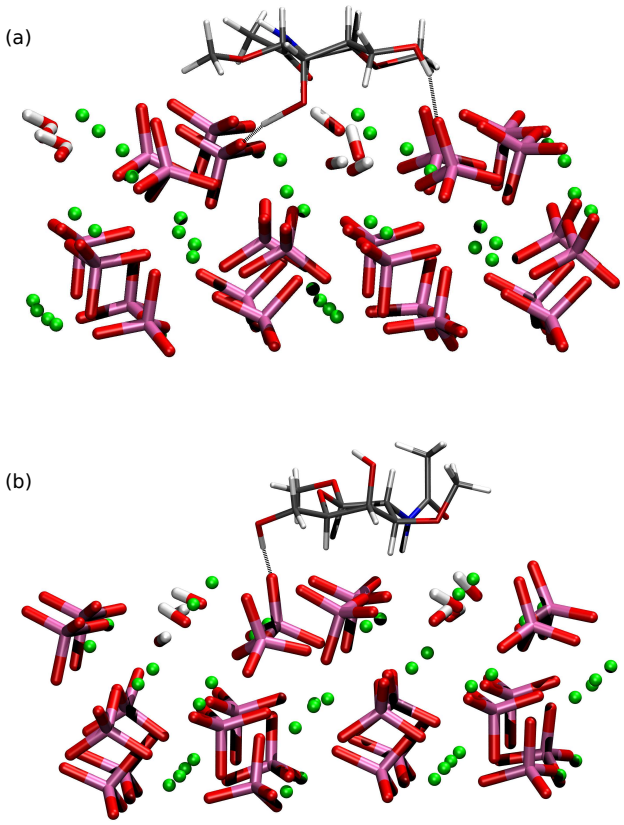

Figure 4: Adsorptions of methylated *N*-acetylgalactosamine on the $(01\bar{1}0)$b surface of hydroxyapatite. (a) orientation I (b) orientation II. Hydrogen bonds from hydroxy groups to phosphate groups are indicated by broken lines (Ca = green, O = red, P = purple, H = white, C = grey, N = blue). These adsorption structures are shown in greater detail in Figures 5c and 5f

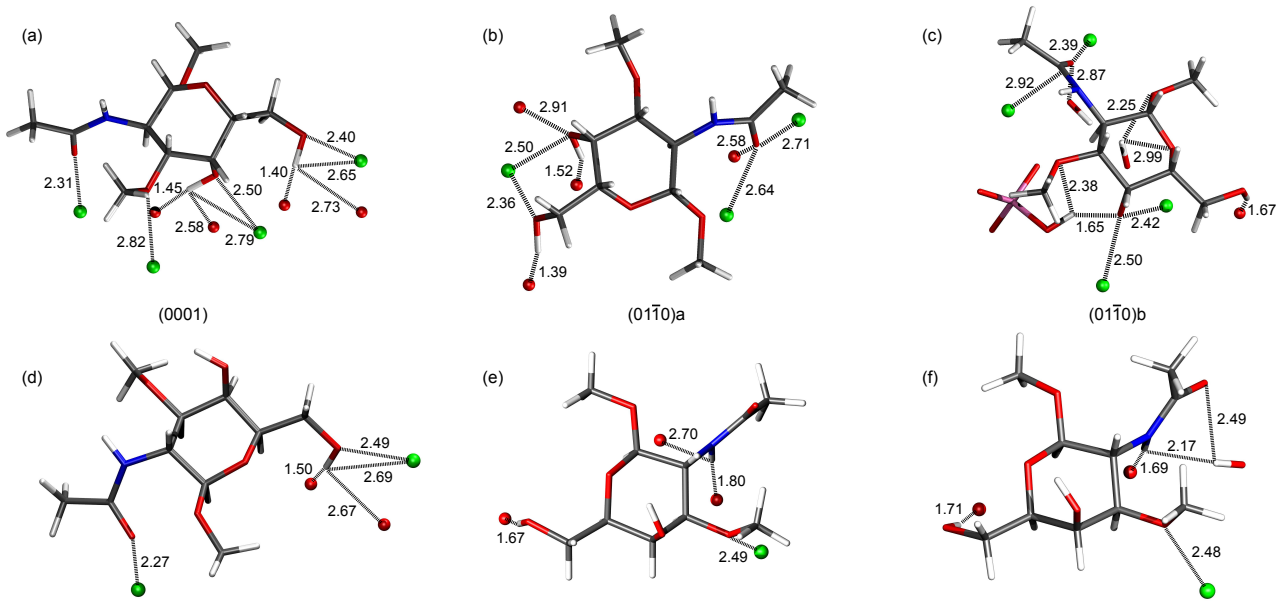

Figure 5: Adsorptions of methylated *N*-acetylgalactosamine on hydroxyapatite. HAP surface atoms are shown if they are within 3 Å of a polar group in the saccharide, and distances are shown in Å. (a) orientation I on (0001) shown in Supplementary Figure 1c, (b) orientation I on (01$\bar{1}$0)a shown in Supplementary Figure 1a, (c) orientation I on (01$\bar{1}$0)b shown in Figure 4a, (d) orientation II on (0001) shown in Supplementary Figure 1d, (e) orientation II on (01$\bar{1}$0)a shown in Supplementary Figure 1b, (f) orientation II on (01$\bar{1}$0)b) shown in Figure 4b (Ca = green, O = red, P = purple, H = white, C = grey, N = blue). Red spheres represent phosphate group oxygens, whereas HAP hydroxy groups are shown in full. In (c) the phosphate group is also shown in full where proton transfer has occurred.

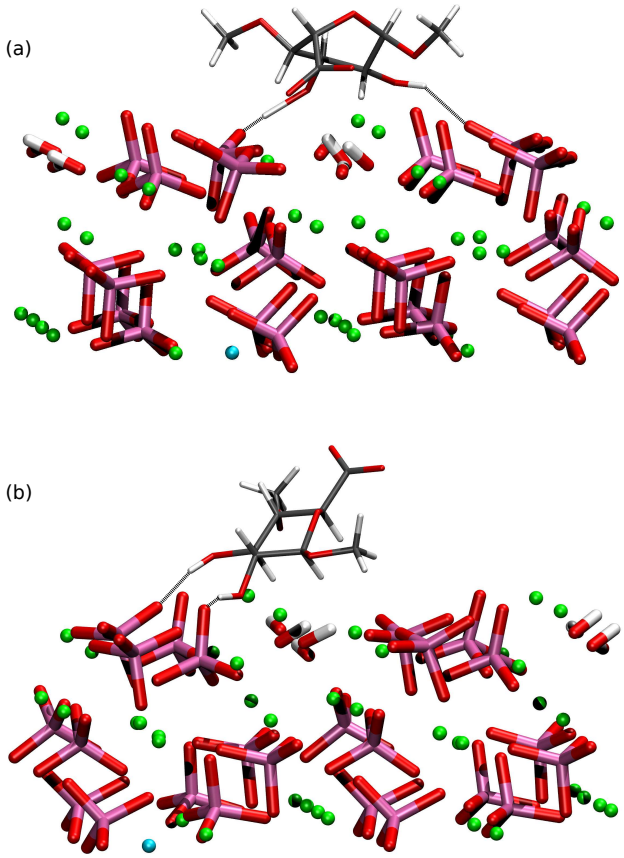

Figure 6: Adsorptions of methylated glucuronic acid on the $(01\bar{1}0)$b surface of hydroxyapatite. (a) orientation I (b) orientation II. Hydrogen bonds from hydroxy groups to phosphate groups are indicated by broken lines (Ca = green, O = red, P = purple, H = white, C = grey). These adsorption structures are shown in greater detail in Figures 7c and 7f

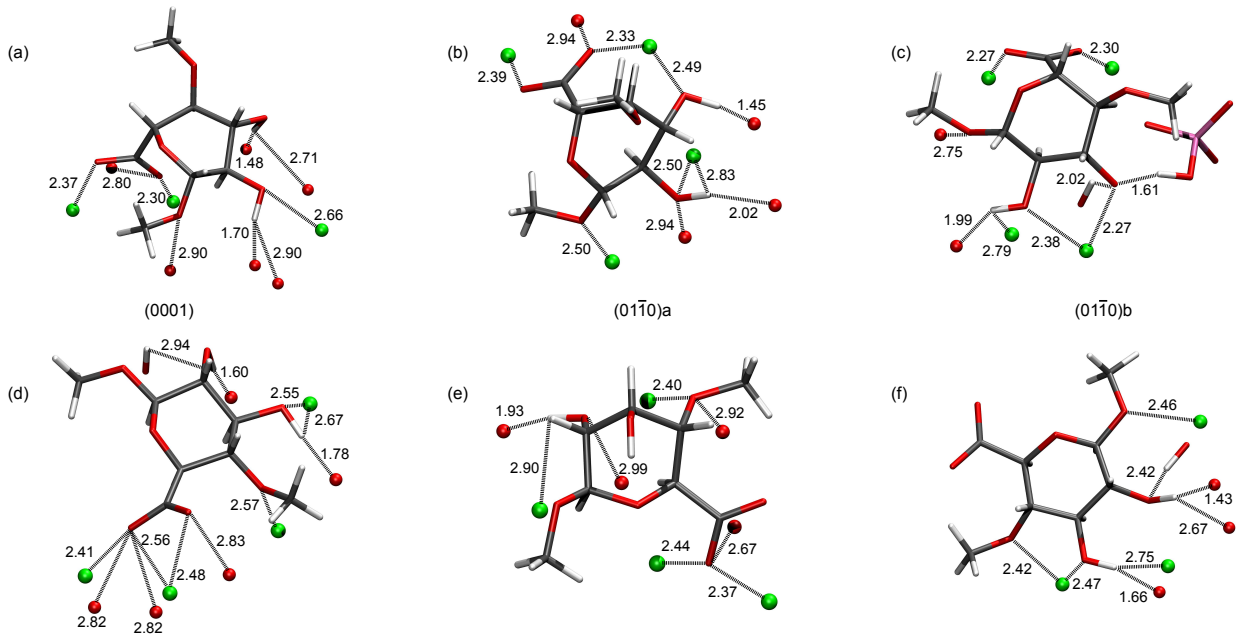

Figure 7: Adsorptions of methylated glucuronic acid on hydroxyapatite. HAP surface atoms are shown if they are within 3 Å of a polar group in the saccharide, and distances are shown in Å. (a) orientation I on (0001) shown in Supplementary Figure 2c, (b) orientation I on (01$\bar{1}$0)a shown in Supplementary Figure 2a, (c) orientation I on (01$\bar{1}$0b shown in Figure 6a, (d) orientation II on (0001) shown in Supplementary Figure 2d, (e) orientation II on (01$\bar{1}$0)a shown in Supplementary Figure 2b, (f) orientation II on (01$\bar{1}$0)b shown in Figure 6b (Ca = green, O = red, P = purple, H = white, C = grey). Red spheres represent phosphate group oxygens, whereas HAP hydroxy groups are shown in full. In (c) the surface phosphate group is also shown in full where proton transfer has occurred.